

Silicon Carbide Supported Liquid Phase (SLP) Hydroformylation Catalysis – Effective Reaction Kinetics from Continuous Gas-phase Operation

Markus Schörner,^[a] Kerstin Mitländer,^[a] Moritz Wolf,^[b] Robert Franke,^[c, d] and Marco Haumann*^[a]

The hydroformylation reaction is one of the most important applications of homogeneous catalysis on an industrial scale with worldwide production capacities exceeding 15 Mio tons per year. Efficient catalyst immobilization becomes mandatory for such large-scale processes. In this work, a supported liquid phase (SLP)-type catalyst on a silicon carbide support material was applied in the continuous Rh-bpp (bpp=biphephos) catalyzed gas-phase hydroformylation of but-1-ene. A parameter variation was carried out in the pressure range from 0.5 to 3.0 bara for but-1-ene, 0.5 to 5 bara for H₂, 0.5 to 5 bara for CO,

and in the temperature range from 90 to 125 °C. Activation energies were determined for the individual reactions showing a shift in activation energy most significantly for the hydroformylation to *n*-pentanal for temperatures of 110 °C and above. For all substrates the effective reaction orders were calculated and employed in a power-law rate model giving good agreement of measured and modeled data within a ±20% error margin. Similar results were obtained using a microkinetic model.

Introduction

Homogeneous catalysis can offer several benefits compared to heterogeneous catalysis. The dissolved complexes, usually modified by appropriate ligands, allow very high specific activity and selectivity at mild reaction conditions.^[1] However, the often tedious separation of the catalyst complex from the reaction mixture hampers the industrial implementation of this type of catalysis. A recent survey on this topic is given in the review article by Vural Gürsel *et al.*^[2] Heterogeneous catalysis, where usually a solid is in contact with a liquid or gas phase, offers significantly simplified product separation and catalyst recycling. Thus, the majority of industrial processes is utilizing heterogeneous catalysts.^[3] A promising approach would be the

combination of both types of catalysis; hence the field of homogeneous catalyst immobilization is being intensively researched and has seen numerous approaches over the past decades.^[4–7] A very promising technique is the concept of supported liquid phase (SLP) catalysis as shown in Figure 1.^[8] Here, a thin film of liquid, containing molecularly dissolved catalyst complexes, is dispersed over the inner surface area of a porous support. Especially ionic liquids exhibit negligible vapor pressures, hence the application of supported ionic liquid phase (SILP) materials allows catalysis in continuous gas-phase processes.^[9] Successful examples include hydroformylation, hydroaminomethylation, carbonylation, water-gas-shift reaction, hydrogenation, and oxychlorination.^[10–24] Besides the high activity and selectivity that is associated with the dedicated

[a] M. Schörner, K. Mitländer, Dr. M. Haumann
Friedrich-Alexander-Universität Erlangen-Nürnberg (FAU)
Lehrstuhl für Chemische Reaktionstechnik (CRT)
Egerlandstr. 3, 91058 Erlangen (Germany)
E-mail: marco.haumann@fau.de

[b] Dr. M. Wolf
Helmholtz Institute Erlangen-Nürnberg for Renewable Energy (IEK-11)
Forschungszentrum Jülich GmbH
Cauerstraße 1, 91058 Erlangen (Germany)

[c] Prof. R. Franke
3 Evonik Operations GmbH
Paul-Baumann-Str. 1, D-45772 Marl (Germany)

[d] Prof. R. Franke
4 Ruhr-Universität Bochum
Lehrstuhl für Theoretische Chemie
Universitätsstr. 150, D-44780 Bochum (Germany)

Supporting information for this article is available on the WWW under <https://doi.org/10.1002/cctc.202200058>

© 2022 The Authors. ChemCatChem published by Wiley-VCH GmbH. This is an open access article under the terms of the Creative Commons Attribution Non-Commercial NoDerivs License, which permits use and distribution in any medium, provided the original work is properly cited, the use is non-commercial and no modifications or adaptations are made.

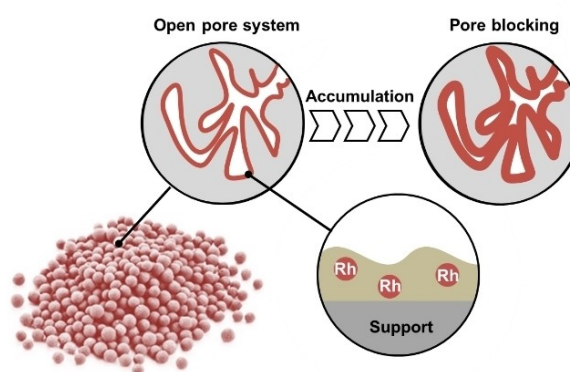
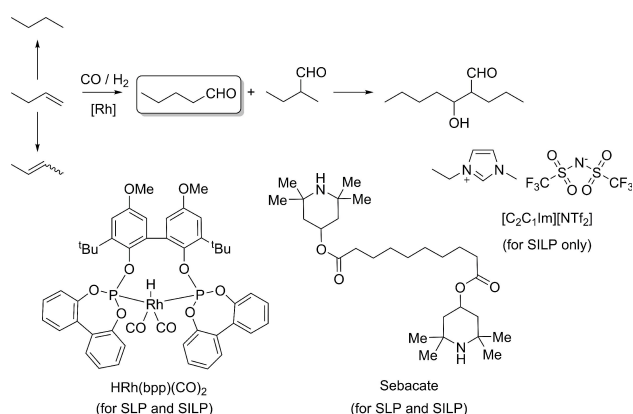


Figure 1. Schematic description of the supported liquid phase (SLP) concept for catalysis. Dissolved hydroformylation catalysts are indicated by “Rh”. Accumulation of substrates or products inside the film leads to pore blocking.

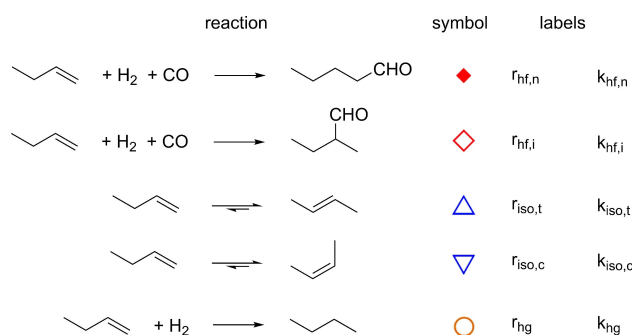
metal-ligand combination used, the stability of such SILP catalysts can be high, exceeding 800 h in academic studies.^[14] However, over such long-term runs, the liquid film can change due to small amounts of substrate or, more likely, product accumulation inside the confined pore space (see Figure 1).

For industrial scenarios, this could result in a slow deactivation due to swelling of the film and blocking of transport pores, which has been observed in e.g. hydroformylation over 2000 h using an Rh-diphosphite-SILP system.^[25] In most cases, regeneration is possible by pressure swing operation.^[10,26] Nevertheless, such interruptions of the process would lower the efficiency and counterbalance the benefits of SILP catalysis. Recently, we published a new SLP-type catalyst, which showed significant improvement over the state of the art SILP-system regarding by-product formation, stability and hence industrial applicability (see Scheme 1).^[15]

It is shown in the study, that no deactivation was observed for the SLP system, while a minor loss of activity was seen in the SILP system. Since the selectivity remained high throughout the run, it was concluded that the well-known effect of pore-blocking by swollen IL films is the reason for the deactivation (schematically depicted in Figure 1). SiC was used as support material since it has an excellent heat conductivity of $120 \text{ W m}^{-1} \text{ K}^{-1}$ compared to $1.38 \text{ W m}^{-1} \text{ K}^{-1}$ for SiO_2 , which is



Scheme 1. Reaction network for the hydroformylation of but-1-ene including undesired by-products. The desired *n*-pentanal is highlighted. Building blocks for SLP and SILP are shown below.



Scheme 2. Reaction network for Rh-bpp-SLP catalyzed hydroformylation of but-1-ene.

commonly used for SILP hydroformylation. Switching to SiC can therefore lower the risk of hot-spot formation in the exothermic reaction when it comes to large-scale applications. In this work, we present kinetic studies of this new and promising SLP catalyst system consisting of Rh-bpp dissolved in sebacate and entrapped within the pore system of SiC particles to gain a better understanding of the system for industry-near applications.

Results and Discussion

Under reaction conditions, the Rh-bpp-SLP catalyst leads to a reaction network of several side reactions (see also Scheme 2). Beyond the desired hydroformylation of but-1-ene and syngas to *n*-pentanal ($r_{\text{hf},n}$), the formation of 2-methylbutanal ($r_{\text{hf},i}$) also occurs. Furthermore, hydrogenation of but-1-ene to butane (r_{hg}) as well as isomerization of but-1-ene to *cis*-2-butene ($r_{\text{iso},c}$) or *trans*-2-butene ($r_{\text{iso},t}$) need to be taken into account. Both isomerization reactions are to be postulated as equilibrium reactions. However, when running the reaction with excessive use of feed to keep the overall conversion of but-1-ene low, equilibrium-posed limitations may be neglected and the assumption of irreversible reactions sufficiently describes the reaction network. As shown in Table S2, the equilibrium conversion for both the formation of *cis*-2-butene and *trans*-2-butene is at 80% or above for a broad temperature and pressure range.

The effective kinetics of each reaction considered was described by the Arrhenius and power-law approach. To examine the activation energies, order of reactions, and rate constants, reliable experimental data were of major importance. Therefore, the stability of the catalyst, the reproducibility of defined reaction conditions, and the independence from the mass of the catalyst had to be checked. The catalyst obtained a steady-state behavior after 30 h TOS (see ESI Figure S2). Periodically checking the reference conditions while performing a partial pressure variation showed no change in activation or selectivity over more than 200 h TOS (see ESI Figure S3). Further investigations using different catalyst loadings showed, that the activity and selectivity were independent of the mass of catalyst used (see ESI Figure S4). Therefore, the overall conversion of but-1-ene scales linearly with the residence time. A metal loading variation from 0.03 to 0.1 wt% was carried out as shown in Figure S5. For all individual reactions, an effective order in Rh concentration of 0.7 was observed. With the value being close to 1, the absence of mass transport limitations can be assumed.

Parameter Estimation

For the determination of the activation energies of the individual reactions, the temperature in the reactor was varied between 90 °C and 130 °C. After calculating the effective reaction rate of every single reaction at stationary conditions, plotting the natural logarithm against the inverse temperature

(Figure 2) allowed the estimation of the effective activation energies according to the Arrhenius approach.

Linear regression of the data points leads to the observation, that the curves were more accurately described by two separate straight lines. Between 105 °C and 110 °C, the correlation of temperature changes, leading to higher activation energies at lower reaction temperatures and vice versa. The determined values are summarized in Table 1.

The effective activation energies determined in the lower temperature range (90–105 °C) are in good agreement with literature data from gradient-free experiments using a similar system. For a Rh-bzp-SILP (bzp = benzpinacol 2,2'-(3,3'-di-tert-butyl-5,5'-dimethoxybiphenyl-2,2'-diyl)bis(oxy)bis(4,4,5,5-tetra-phenyl-1,3,2-dioxaphospholan), sebacate, [C₂C₁Im][NTf₂]) catalyst an effective activation energy of 55.7–65.2 kJ mol⁻¹ was determined for the formation of *n*-pentanal.^[28] At temperatures above 105 °C, especially the formation of the desired *n*-pentanal was notably influenced by temperature. The effective activation energy changed from 51.6 kJ mol⁻¹ to an extremely low value of

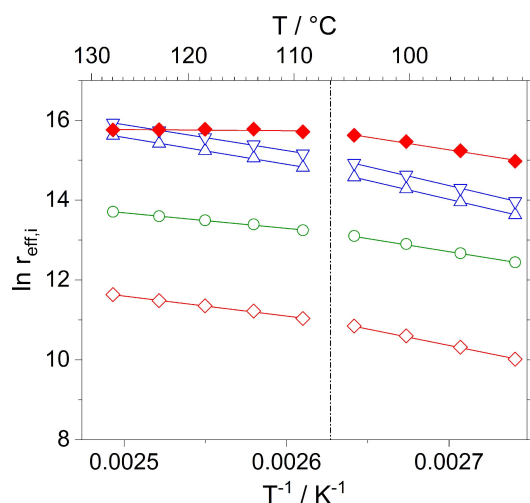


Figure 2. Rh-bpp-SLP catalyzed hydroformylation of but-1-ene. Arrhenius plot derived from temperature variation experiments ($T_{\text{reactor}} = 90\text{--}125\text{ }^{\circ}\text{C}$) for Rh-SLP catalyzed hydroformylation of but-1-ene. Individual reaction rates $r_{\text{eff},i}$ were calculated for the formation of *n*-pentanal (\blacklozenge), 2-methylbutanal (\blacklozenge), *cis*-2-butene (\blacktriangledown), *trans*-2-butene (\blacktriangle) and butane (\circ). The dashed line indicates the estimated temperature (ca. 107 °C), at which the SLP system becomes mass transfer influenced. Reaction conditions: $m_{\text{catalyst}} = 1.0\text{ g}$, $w_{\text{Rh}} = 0.05\text{ wt\%}$, Rh:bpp = 1 : 4 (molar), bpp:sebacate = 1 : 4 (molar), $p = 10\text{ bara}$, $\dot{n}_{\text{H}_2} = 4.6\text{ mmol min}^{-1}$, $\dot{n}_{\text{CO}} = 4.1\text{ mmol min}^{-1}$, $\dot{n}_{\text{inert}} = 2.2\text{ mmol min}^{-1}$, $\dot{n}_{\text{but-1-ene}} = 1.6\text{ mmol min}^{-1}$.

2.2 kJ mol⁻¹. We assume that a complex interplay between classical macro-kinetics (diffusion vs reaction rate) and solubility inside the film is responsible for this decline. Only taking the data points above 110 °C into account even resulted in a slightly negative effective activation energy of -2 kJ mol^{-1} for the formation of *n*-pentanal. A similar decrease in activity with increasing temperatures has been reported for a SILP system in the nickel catalyzed dimerization of propene. In that case, a decrease in propene solubility with higher temperature was the cause.^[30] In our case, the behavior probably also stems from an substrate impoverishment in the supported liquid phase. As only the formation of *n*-pentanal is strongly effected, an impoverishment of syngas is assumed. Some evidence in support of this hypothesis will be briefly outlined below. Since no literature data of but-1-ene, CO and H₂ solubility in bis(2,2,6,6-tetramethyl-4-piperidyl) sebacate is reported, calculations of the Henry coefficients were conducted using COSMOthermX19 (ESI Figure S18). It is found, that the solubility of but-1-ene exceeds the syngas solubility by far, making an impoverishment of but-1-ene very unlikely. For H₂ and CO solubility, a decreasing solubility with increasing temperature is found from theoretical calculations (see ESI Figure S18). For CO this trend could be also observed experimentally (see ESI Figure S19). These trends are in accordance with measurements from Ohlin *et al.* and Sharma *et al.* for ionic liquids in the temperature range up to 80 °C and 100 °C respectively.^[31,32]

To characterize the influence of the individual reactants on the reaction network and thereby determine the effective reaction orders, partial pressures of the components in the feed were varied. While the concentration of one substrate in the feed was changed, the partial pressures of the other two reactants were kept constant. During the feed variations, an inert component was added to maintain the feed volume flow as well as the total pressure of 10 bara in the reactor.

The partial pressure of but-1-ene was varied between 0.5 bara and 3 bara. The linearized results are shown in Figure 3. The reaction orders were estimated by the slope of the straight lines fitted to the data (see Table 2 for details). Since but-1-ene participated in every considered reaction, its concentration positively influenced all reactions, resulting in reaction orders of 1.1–1.2.

The partial pressures of hydrogen and carbon monoxide were varied each between 0.5 bara and 5 bara and their influence was evaluated after linearization (see Figure 4). The formation of *n*-pentanal as a function of H₂ partial pressure

Table 1. Effective activation energies determined in the temperature range from 90 to 130 °C.

Compound	i	90–105 °C	110–130 °C	40–100 °C ^[a]	95–115 °C ^[b]
		$E_{A,i}$ [kJ mol ⁻¹]			
<i>n</i> -pentanal	<i>n</i>	51.6	2.2	55.7–65.2	30.3
2-methylbutanal	<i>iso</i>	66.2	40.5	42.7–48.3	56.7
<i>cis</i> -2-butene	<i>cis</i>	77.2	52.5	74.1–79.2	49.1–58.2
<i>trans</i> -2-butene	<i>trans</i>	76.4	54.5	85.4–92.6	
butane	<i>hy</i>	52.8	31.4	54.1–57.4	64.2

[a] Results from Kokolakis using a Rh-SILP catalyst in the continuous gas-phase hydroformylation of but-1-ene,^[28] [b] Results from Jörke *et al.* using a Rh-bpp-complex in the liquid-phase hydroformylation of *n*-decenes.^[29]

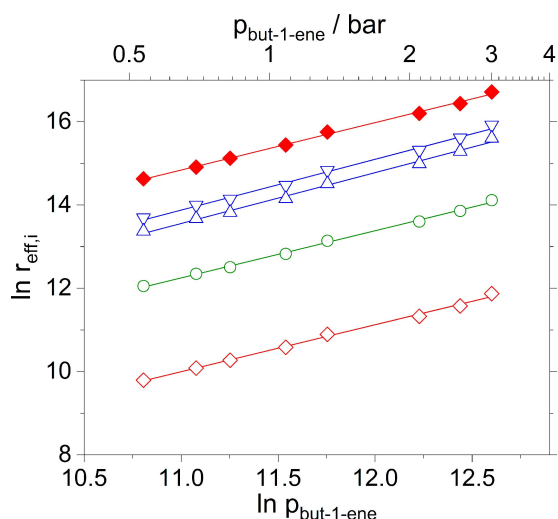


Figure 3. Rh-bpp-SLP catalyzed hydroformylation of but-1-ene. Differential analysis of reaction rate as a function of but-1-ene partial pressure. Individual reaction rates $r_{\text{eff},i}$ were calculated for the formation of *n*-pentanal (\blacklozenge), 2-methylbutanal (\blacklozenge), *cis*-2-butene (\blacktriangledown), *trans*-2-butene (\blacktriangle) and butane (\circ). Temperature = 100 °C, pressure range: 0.5 to 3.0 bara for but-1-ene. Reaction conditions: $m_{\text{catalyst}} = 1.0$ g, $w_{\text{Rh}} = 0.05$ wt%, Rh:bpp = 1:4 (molar), bpp:sebacate = 1:4 (molar), $p = 10$ bara, $T = 100$ °C, $\dot{n}_{\text{H}_2} = 4.6$ mmol min⁻¹, $\dot{n}_{\text{CO}} = 4.1$ mmol min⁻¹.

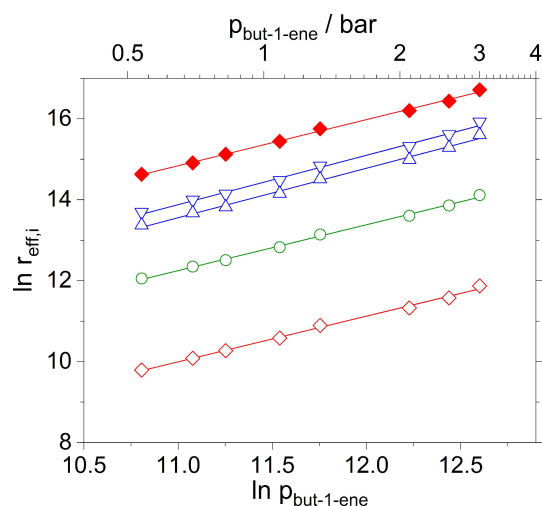


Figure 4. Rh-bpp-SLP catalyzed hydroformylation of but-1-ene. Differential analysis of reaction rate as a function of H₂ (top) and CO (bottom) partial pressure. Individual reaction rates $r_{\text{eff},i}$ were calculated for the formation of *n*-pentanal (\blacklozenge), 2-methylbutanal (\blacklozenge), *cis*-2-butene (\blacktriangledown), *trans*-2-butene (\blacktriangle) and butane (\circ). Temperature = 100 °C, pressure ranges: 0.5 to 5 bara for H₂, and 0.5 to 5 bara for CO. Reaction conditions: $m_{\text{catalyst}} = 1.0$ g, $w_{\text{Rh}} = 0.05$ wt%, Rh:bpp = 1:4 (molar), bpp:sebacate = 1:4 (molar), $p = 10$ bara, $T = 100$ °C, $\dot{n}_{\text{but-1-ene}} = 1.6$ mmol min⁻¹.

Table 2. Obtained effective reaction orders of but-1-ene, CO, and H₂ in each reaction.

Compound	index	$n_{\text{but-1-ene}}/-$	$n_{\text{CO}}/-$	$n_{\text{H}_2}/-$
<i>n</i> -pentanal	<i>n</i>	1.1	0.8	0.3 ^[a]
2-methylbutanal	<i>iso</i>	1.1	0.9	-0.1
<i>cis</i> -2-butene	<i>cis</i>	1.2	-0.2	0.0
<i>trans</i> -2-butene	<i>trans</i>	1.2	-0.2	0.0
butane	<i>hy</i>	1.1	-0.3	0.9

[a] only partial pressures higher than 2 bar considered.

could not sufficiently be described by linear regression over the total pressure range studied. When partial pressures below 2 bar were excluded, a linear trend was obtained as seen in Figure 4, resulting in an effective order of 0.3. When decreasing the partial pressure below 2 bar, the effective reaction order increased to values around 1. This value supports the occurrence of a mass transport controlled system as mass transport is proportional to the driving force. The most significant influence of hydrogen could be observed in the hydrogenation reaction with a reaction order of 0.8. The isomerization reactions and the formation of 2-methylbutanal were almost unaffected by the H₂-concentration in the feed, which resulted in reaction orders of 0.1 and 0.0, respectively. The hydroformylation leading to *n*-pentanal was described with a positive reaction order of 0.3.

Observing the CO-variations, the hydrogenation of but-1-ene and both isomerization reactions were negatively influenced by higher CO concentrations. In contrast, the hydroformylation forming either *n*-pentanal or 2-methylbutanal showed a positive order in CO, reaching 0.8 and 0.9, respectively. This positive influence contradicts formerly re-

ported results for SILP systems, dealing with the hydroformylation of but-1-ene using Rh-bzp-complexes as catalysts ([C₂C₁im][NTf₂] based).^[28,33] For a Rh-bpp-complex Jörke *et al.* reported a positive effect of CO in the hydroformylation of decene while the isomerization reaction decreases, when increasing the overall syngas pressure.^[29] Using oleonitrile as substrate in the Rh-bpp catalyzed hydroformylation, also Le Goanvic *et al.* report a positive effect of CO when syngas composition is changed from H₂:CO of 1:1 to 1:4 at 10 bar.^[34] A comparison experiment using a SILP-Rh-bpp catalyst ([C₂C₁im][NTf₂] as ionic liquid) showed a similar positive trend for the hydroformylation reactions (0.7 for *n*-pentanal, 0.5 for 2-methylbutanal) while a negative effective reaction order was observed for all side reactions (see Supporting Information). These negative effective reaction orders of the side reactions possibly stem from pre-equilibrium steps resulting in a shift from active hydrido-carbonyl complex to inactive Rh-species at higher CO partial pressures.^[35-37] Table 2 summarizes the observed effective reaction orders.

Similar values for effective reaction orders and activation energies have been measured on a larger scale using a SiC-monolith based SLP catalyst (~100 g support) (see ESI Table S3).^[15] The system showed a similar behavior at low hydrogen partial pressures and an almost identical drop of the effective activation energy above 105 °C. The similarity of 1 g and 100 g approach indicates, that the reported findings stem from the intrinsic properties of the catalyst rather than the scaling size.

Model Development

Numerous kinetic models have been tested in literature for long and short-chain olefin hydroformylation,^[29,35,38–41] while less models are published for SILP-catalyzed hydroformylation of short-chain olefins.^[20,28] Here, we compare a power-law approach (model 1) using the experimentally obtained effective reaction orders and one microkinetic model (model 2).

The microkinetic model was developed using the methodology from Christiansen.^[42,43] Starting from a reaction cycle, this formalism provides a mathematical description of every reaction step in one equation. Assumptions can be used to simplify the obtained equation. Here, the following reaction cycle was used.

Starting from I, the active state II is formed by CO-elimination, while possible side formations are either the formation of a Rh-dimer (Ia) or the formation of a tetracarbonyl complex (Ib) by CO-addition with or without H₂-elimination. Complex II can coordinate an olefin to result in complex III. To achieve the desired product *n*-pentanal, olefin-addition in α -position followed by CO-insertion and oxidative addition of H₂ is required. Finally, reductive elimination of the linear aldehyde takes place to yield complex II again. As no inhibition of the hydroformylation reaction caused by CO was determined experimentally, a possible formation of a dicarbonyl species from species V_{hy} was not taken into account to minimize the complexity of the model. The same steps are required to form the branched C₅-aldehyde except the olefin addition takes place in β -position (not shown). This addition is also required to achieve one of the two 2-butene isomers going from III to IV_{iso}. Following β -olefin coordination and elimination, either *trans*-2-butene or *cis*-2-butene are obtained as products. The hydrogenation can either take place from the olefin addition in α - or β -position. As a simplification, only the hydrogenation of but-1-ene after α -addition is assumed. In addition to the stated irreversible reaction steps, state II was assumed to be the most abundant catalyst species (MACS). This assumption is supported by Jörke *et al.* who showed for a similar Rh-bpp-complex that the olefin coordination is the RDS.^[29,43,45,46]

In contrary to model 1, the microkinetic model cannot account for the inhibiting effect of increasing CO partial pressures leading to inactive Rh-species (I, Ia, Ib). To overcome this, an upstream equilibrium equation of I and II is used to determine the active Rh-complexes depending on the reaction conditions (Equation 1 [Eq. (1)]).^[40]

$$\frac{n_{\text{cat,I}}}{n_{\text{cat,II}} p_{\text{CO}}} = \frac{m_{\text{cat,I}}}{m_{\text{cat,II}} p_{\text{CO}}} = K_{\text{eq,cat}} \quad (1)$$

By doing so, the total amount of catalyst in the system is divided into an active species and an inactive species (Equation 2 [Eq. (2)]).

$$m_{\text{cat,total}} = m_{\text{cat,I}} + m_{\text{cat,II}} \quad (2)$$

Therefore, to take the changing amount of active species into account, an additional factor according to Equation 3 [Eq. (3)] is introduced in model 2.

$$m_{\text{cat,II}} = \frac{m_{\text{cat,total}}}{1 + K_{\text{eq,cat}} p_{\text{CO}}} \quad (3)$$

The resulting rate equations for all models and all reactions are summarized in Equations 6–11 [Eqs. (4–9)]. The missing characteristic parameters were fitted using a data set of 38 different pressure settings and tested with 10 additional pressure settings. All measurements were carried out at 100 °C, therefore no temperature dependency is given in the models. The substrate pressures ranges were from 0.5 to 3.0 bara for but-1-ene, 2.0 to 5 bara for H₂, and 0.5 to 5 bara for CO to exclude possible mass transport influence as seen at low hydrogen pressure.

Hydroformylation:

$$r_{1,i} = k_{1,i} p_{\text{but-1-ene}}^{\text{a,i}} p_{\text{CO}}^{\text{b,i}} p_{\text{H}_2}^{\text{c,i}} \quad (4)$$

i = *n*-pentanal und 2-methylbutanal

$$r_{2,i} = \frac{1}{1 + K_{2,\text{eq,cat}} p_{\text{CO}}} \frac{k_{2,i} p_{\text{but-1-ene}} p_{\text{CO}} p_{\text{H}_2}}{1 + K_{2\text{a},i} p_{\text{H}_2} + K_{2\text{b},i} p_{\text{H}_2} p_{\text{CO}}} \quad (5)$$

i = *n*-pentanal(*n*) und 2-methylbutanal(*iso*)

Isomerization:

$$r_{1,i} = k_{1,i} \left(p_{\text{but-1-ene}}^{\text{a,i}} - \frac{p_i}{K_{\text{eq},i}} \right) p_{\text{CO}}^{\text{b,i}} p_{\text{H}_2}^{\text{c,i}} \quad (6)$$

i = *cis*-2-butene und *trans*-2-butene

$$r_{2,i} = \frac{1}{1 + K_{2,\text{eq,cat}} p_{\text{CO}}} k_{2,i} \left(p_{\text{but-1-ene}} - \frac{p_i}{K_{\text{eq},i}} \right) \quad (7)$$

i = *cis*-2-butene und *trans*-2-butene

Hydrogenation:

$$r_{1,i} = k_{1,i} p_{\text{but-1-ene}}^{\text{a,i}} p_{\text{CO}}^{\text{b,i}} p_{\text{H}_2}^{\text{c,i}} \quad (8)$$

i = butane

$$r_{2,i} = \frac{1}{1 + K_{2,\text{eq,cat}} p_{\text{CO}}} \frac{k_i p_{\text{but-1-ene}} p_{\text{H}_2}}{1 + K_{2,i} p_{\text{H}_2}} \quad (9)$$

i = butane

Using the experimental data set, the rate constants *k*_{1,*i*} for the power-law approach were fitted. The resulting parity plot is shown in Figure 5. All data was within $\pm 20\%$ error for the tested pressure range. Overall, the hydroformylation to *n*-pentanal showed the highest variation. Also, the validation set shows a good agreement of model and experimental data as shown in Figure 6.

Similarly, the unknown reaction parameters were fitted for the microkinetic model using the training set (see Figure 7). Noteworthy, a lowered amount of parameters was used to describe the reaction rates compared to the power-law approach. Nevertheless, the microkinetic model which assumes

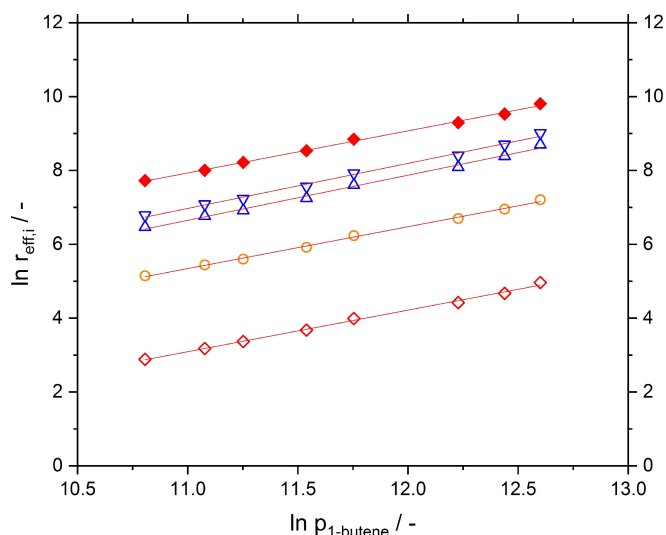


Figure 5. Parity plot (left) and relative errors (right) for training set of model 1. Individual reaction rates $r_{\text{eff},i}$ were calculated for the formation of n-pentanal (\blacklozenge), 2-methylbutanal (\blacklozenge), cis-2-butene (∇), trans-2-butene (\triangle) and butane (\circ). Temperature = 100 °C, pressure ranges: 0.5 to 3.0 bara for but-1-ene, 2 to 5 bara for H_2 , and 0.5 to 5 bara for CO.

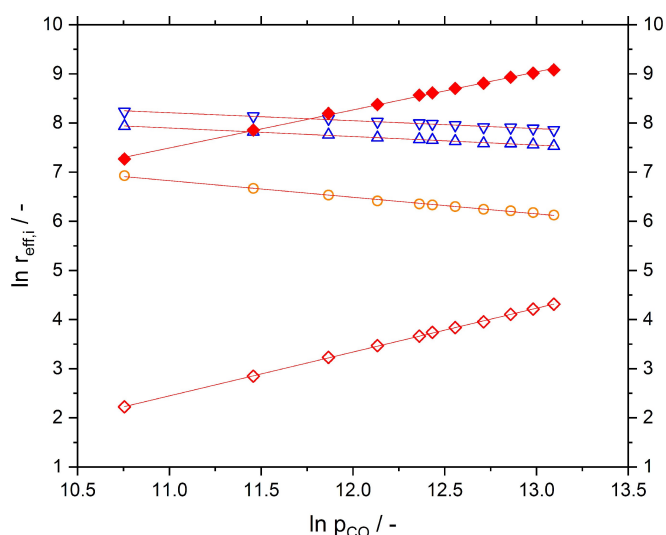


Figure 6. Parity plot (left) and relative errors (right) for validation set of model 1. Individual reaction rates $r_{\text{eff},i}$ were calculated for the formation of n-pentanal (\blacklozenge), 2-methylbutanal (\blacklozenge), cis-2-butene (∇), trans-2-butene (\triangle) and butane (\circ). Temperature = 100 °C, pressure ranges: 0.5 to 3.0 bara for but-1-ene, 2 to 5 bara for H_2 , and 0.5 to 5 bara for CO.

complex II to be the most abundant catalyst species allows good agreement of model and simulation (see Figure 8).

Table 3 summarizes the fitted reaction rate parameters including the standard deviations.

Conclusion

In the present work, a reaction parameter variation using a recently published supported liquid phase (SLP)-type catalyst

Table 3. Fitted reaction rate parameters using ACM for model 1 (index 1, power-law approach) and model 2 (index 2, microkinetic approach with complex II as MACS).

Parameter	Unit	Value	Standard deviation
$k_{1,n}$	$\text{mol h}^{-1} \text{kg}_{\text{Rh}}^{-1} \text{bar}^{-2.2}$	1304520	21727
$k_{1,\text{iso}}$	$\text{mol h}^{-1} \text{kg}_{\text{Rh}}^{-1} \text{bar}^{-1.9}$	15444	207
$k_{1,\text{cis}}$	$\text{mol h}^{-1} \text{kg}_{\text{Rh}}^{-1} \text{bar}^{-1}$	2606310	25429
$k_{1,\text{trans}}$	$\text{mol h}^{-1} \text{kg}_{\text{Rh}}^{-1} \text{bar}^{-1}$	1888800	21087
$k_{1,\text{hy}}$	$\text{mol h}^{-1} \text{kg}_{\text{Rh}}^{-1} \text{bar}^{-1.7}$	174416	1655
$K_{2,\text{eq,cat}}$	bar^{-1}	0.1315	0.0054
$k_{2,n}$	$\text{mol h}^{-1} \text{kg}_{\text{Rh}}^{-1} \text{bar}^{-3}$	1490000	387323
$k_{2,\text{iso}}$	$\text{mol h}^{-1} \text{kg}_{\text{Rh}}^{-1} \text{bar}^{-3}$	365141	114773
$k_{2,\text{cis}}$	$\text{mol h}^{-1} \text{kg}_{\text{Rh}}^{-1} \text{bar}^{-1}$	3250000	60273
$k_{2,\text{trans}}$	$\text{mol h}^{-1} \text{kg}_{\text{Rh}}^{-1} \text{bar}^{-1}$	2360000	47729
$k_{2,\text{hy}}$	$\text{mol h}^{-1} \text{kg}_{\text{Rh}}^{-1} \text{bar}^{-2}$	167483	17837
$K_{2a,n}$	bar^{-1}	0.3491	0.1543
$K_{2b,n}$	bar^{-2}	0.0074	0.0174
$K_{2a,\text{iso}}$	bar^{-1}	19.61	6.852
$K_{2b,\text{iso}}$	bar^{-2}	0.0000	0.2164
$K_{2,\text{hy}}$	bar^{-1}	0.0000	0.0251

for the gas-phase hydroformylation of but-1-ene was carried out. At first, the stability of the Rh-bpp-complex was shown, and a temperature variation was done. Using the Arrhenius approach the activation energy for the individual reactions hydroformylation to n-pentanal, hydroformylation to 2-methylbutanal, isomerization to *cis*-2-butene, isomerization to *trans*-2-butene, and hydrogenation to butane were determined. For temperatures of 105 °C and below, they show good agreement with the literature. For temperatures of 110 °C and above, a shift in activation energy was measured being most significant for n-pentanal (51.6 kJ mol^{-1} at $< 105^\circ\text{C}$, 2.2 kJ mol^{-1} at $> 110^\circ\text{C}$). Next, a pressure variation of the substrates was carried out showing a strongly positive effective reaction order of CO in the hydroformylation reactions (0.8 for n-pentanal, 0.9 for 2-methylbutanal) while a negative effective reaction order for the other reactions was measured. This is contrary to former findings with comparable SILP hydroformylation catalysts.^[28,33] Literature using Rh-bpp in liquid phase also showed a positive influence of CO partial pressure.^[29,34] The obtained effective reaction orders were used in a rate model using the power-law approach. A training set of pressure settings at 100 °C was used to fit the unknown rate constants, and the model was tested using additional pressure settings. A good agreement of measurements and model was obtained within a $\pm 20\%$ range. Similar results were obtained using a microkinetic model based on Christiansen's methodology when assuming the complex II (Scheme 3) to be the most abundant catalyst species (MACS). With the kinetics data documented here, it will be possible in the future to fine-tune designs for reactors containing SLP systems to immobilize catalysts for hydroformylation. Based on this, it will be possible to design corresponding large-scale processes. This could make it possible to provide significantly more sustainable processes for hydroformylation in the future, in which greenhouse gas emissions are significantly reduced. Savings of 50% compared to standard liquid-phase processes seem possible.^[47]

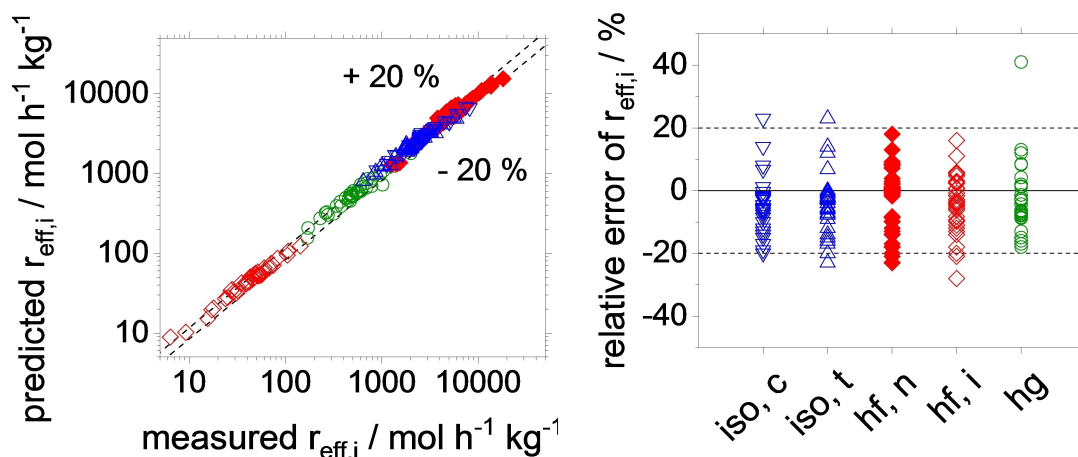


Figure 7. Parity plot (left) and relative errors (right) for training set of model 2. Individual reaction rates $r_{\text{eff},i}$ were calculated for the formation of n-pentanal (♦), 2-methylbutanal (◊), cis-2-butene (▽), trans-2-butene (△) and butane (○). Temperature = 100 °C, pressure ranges: 0.5 to 3.0 bara for but-1-ene, 2 to 5 bara for H_2 , and 0.5 to 5 bara for CO.

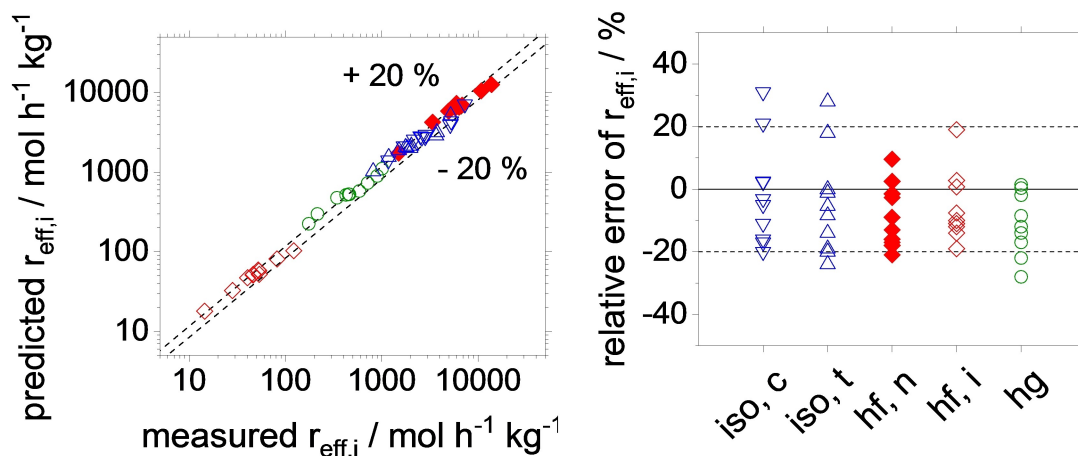


Figure 8. Parity plot (left) and relative errors (right) for validation set of model 2. Individual reaction rates $r_{\text{eff},i}$ were calculated for the formation of n-pentanal (♦), 2-methylbutanal (◊), cis-2-butene (▽), trans-2-butene (△) and butane (○). Temperature = 100 °C, pressure ranges: 0.5 to 3.0 bara for but-1-ene, 2 to 5 bara for H_2 , and 0.5 to 5 bara for CO.

Experimental Section

The SiC-support was already used in former catalytic studies in a monolithic form.^[15] Due to the large particle size and hence the high Rh-loading, this geometry is rather unsuitable for detailed kinetic studies. Therefore, the monolith was crushed, to prepare an SLP powder catalyst via wet impregnation. The resulting powder was sieved to achieve a particle size fraction of 200–500 μm to ensure the absence of pore diffusion influence.^[27] The crushed monolith pieces were calcinated for 6 h at 600 °C in air and stored in a glovebox afterward. (More detailed information about the support and its preparation can be found in the ESI.)

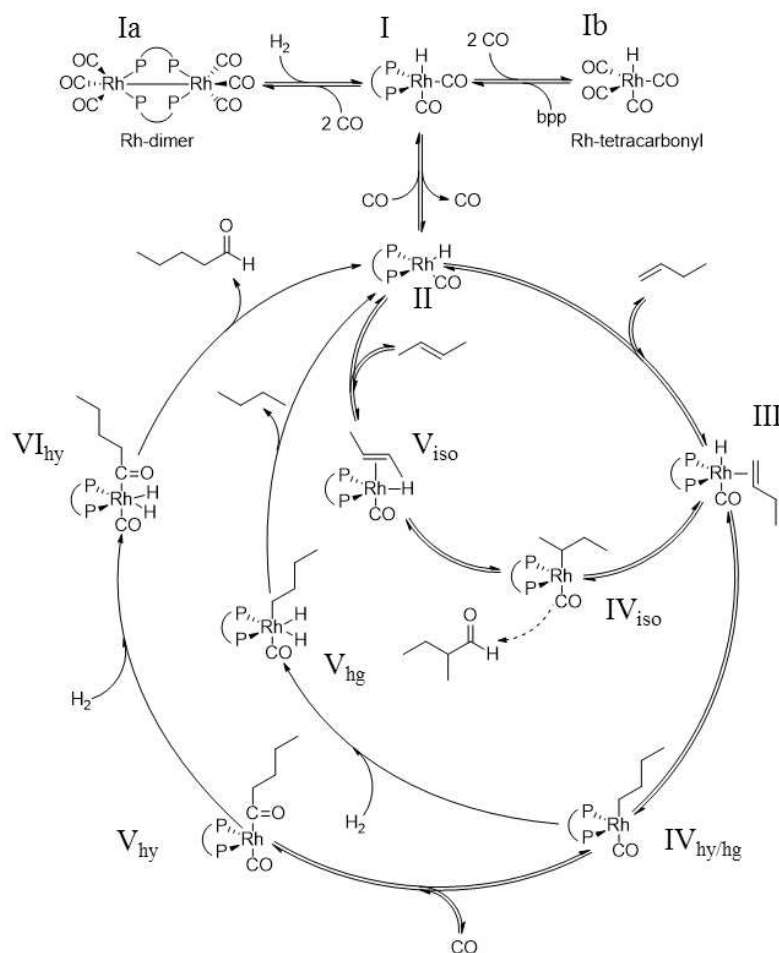
The preparation of the SLP catalyst took place under inert conditions. In a glovebox, the Rh-precursor $\text{Rh}(\text{acac})(\text{CO})_2$ (Sigma-Aldrich) was added to achieve a weight loading of Rh of 0.05% according to Equation 10 [Eq. (10)].

$$w_{\text{Rh}} = \frac{m_{\text{Rh}}}{m_{\text{support}}} \quad (10)$$

Next, the ligand 6,6'-[(3,3'-Di-tert-butyl-5,5'-dimethoxy-1,1'-biphenyl-2,2'-diyl)bis(oxy)]bis(dibenzo[d,f][1,3,2]dioxaphosphin) (biphenos = bpp, Evonik Operations GmbH) and the additive bis(2,2,6,6-tetramethyl-4-piperidyl) sebacate were added in a molar ratio to Rh of 1:4 and 1:16 in a Schlenk flask. Using these ratios, a theoretical pore filling degree of 20 vol% was achieved according to Equation 11 [Eq. (11)]. The liquid density at 100 °C of the operando formed sebacate-liquid phase was measured to be approximately 1 g ml^{-1} .

$$\alpha_{\text{IL}} = \frac{V_{\text{IL}}}{V_{\text{pore}}} \quad (11)$$

Finally, the support was added. Using the Schlenk-technique, 30 ml oxygen-free and water-free dichloromethane (Sigma-Aldrich) was added to dissolve the catalyst complex and the additive. The solution was mixed to ensure a proper dissolution of all the components. Complex formation was monitored by means of high pressure solution NMR.^[48] Afterward, the dichloromethane (DCM) was removed using an inertized rotary evaporator at 50 rpm and



Scheme 3. Reaction cycle of SLP-catalyzed hydroformylation of but-1-ene. Also shown: isomerization to 2-butene and hydrogenation to butane.^[29,40,44]

800 mbar for 1 h. The heating bath was set to 42 °C. After evaporation of the liquid and obtaining a free-flowing powder, the vacuum was set to 5 mbar for additional 30 minutes to remove all solvent from the porous system. The catalyst was then stored in the glovebox until usage. For the comparison experiment using a SILP-catalyst the IL [C2C1m][NTf2] was added to the Schlenk-flask instead of the additive. This IL was used because it is able to readily dissolve the Rh-bpp complex. Due to its hydrophobic nature, it also prevents hydrolysis of the bpp-ligand. Hence, it is the benchmark IL for gas-phase hydroformylation with Rh-bpp SILP-catalysts.

Acknowledgements

The authors gratefully acknowledge financial support from the European Commission within the Horizon2020-SPIRE project MACBETH (grant agreement number 869896) and the Deutsche Forschungsgemeinschaft (DFG, German Research Foundation) – Project-ID 431791331 – SFB 1452 (CLINT). The authors thank the project partners LiqTech Holding A/S for supply of support material, Morten Logemann (RWTH Aachen, Germany) for membrane coating of the monolith and Jakob Maximilian Marinkovic (DTU, Denmark) for catalytic impregnation of the membrane

coated monolith. Open Access funding enabled and organized by Projekt DEAL.

Conflict of Interest

The authors declare no conflict of interest.

Data Availability Statement

The data that support the findings of this study are available from the corresponding author upon reasonable request.

Keywords: diphosphite ligand · hydroformylation · immobilization · rhodium · supported catalysts

- [1] P. W. Van Leeuwen, in *Homogeneous Catalysis – Understanding the Art*, Kluwer Academic Publishers, Dordrecht, The Netherlands, **2004**.
- [2] I. Vural Gürsel, T. Noël, Q. Wang, V. Hessel, *Green Chem.* **2015**, *17*, 2012–2026.
- [3] S. Bhaduri, D. Mukesh, in *Homogeneous Catalysis – Mechanisms and Industrial Applications*, John Wiley & Sons, Hoboken, New Jersey, **2000**.

- [4] *Regulated Systems for Multiphase Catalysis*, (Eds: W. Leitner, M. Hölscher), Springer Berlin, Heidelberg, Germany **2008**.
- [5] J. C. Bailar, *Catal. Rev.* **2006**, *10*, 17–36.
- [6] *Catalyst Separation, Recovery and Recycling*, (Eds: D. J. Cole-Hamilton, R. P. Tooze), Springer, Dordrecht, The Netherlands **2006**.
- [7] *Multiphase Homogenous Catalysis*, (Eds: B. Cornils, W. A. Herrmann, I. T. Horváth, W. Leitner, S. Mecking, H. Olivier-Bourbigou, D. Vogt), Wiley-VCH, Weinheim, **2005**.
- [8] J. M. Herman, A. P. A. F. Rocourt, P. J. Van den Berg, P. J. Van Krugten, J. J. F. Scholten, *Chem. Eng. J.* **1987**, *35*, 83–103.
- [9] *Supported Ionic Liquids – Fundamentals and Applications*, (Eds: R. Fehrmann, A. Riisager, M. Haumann) Wiley-VCH, Weinheim, **2014**.
- [10] M. Haumann, M. Jakuttis, S. Werner, P. Wasserscheid, *J. Catal.* **2009**, *263*, 321–327.
- [11] U. Hintermair, G. Francio, W. Leitner, *Chemistry* **2013**, *19*, 4538–4547.
- [12] U. Hintermair, T. Höfener, T. Pullmann, G. Francio, W. Leitner, *ChemCatChem* **2010**, *2*, 150–154.
- [13] U. Hintermair, C. Roosen, M. Kaever, H. Kronenberg, R. Thelen, S. Aey, W. Leitner, L. Greiner, *Org. Process Res. Dev.* **2011**, *15*, 1275–1280.
- [14] M. Jakuttis, A. Schonweiz, S. Werner, R. Franke, K. D. Wiese, M. Haumann, P. Wasserscheid, *Angew. Chem. Int. Ed. Engl.* **2011**, *50*, 4492–4495.
- [15] M. Logemann, J. M. Marinkovic, M. Schörner, E. José García-Suárez, C. Hecht, R. Franke, M. Wessling, A. Riisager, R. Fehrmann, M. Haumann, *Green Chem.* **2020**, *22*, 5691–5700.
- [16] E. Öchsner, M. J. Schneider, C. Meyer, M. Haumann, P. Wasserscheid, *Appl. Catal. A* **2011**, *399*, 35–41.
- [17] A. Riisager, R. Fehrmann, S. Flicker, R. van Hal, M. Haumann, P. Wasserscheid, *Angew. Chem. Int. Ed. Engl.* **2005**, *44*, 815–819.
- [18] A. Riisager, B. Jorgensen, P. Wasserscheid, R. Fehrmann, *Chem. Commun.* **2006**, 994–996.
- [19] M. J. Schneider, M. Lijewski, R. Woelfel, M. Haumann, P. Wasserscheid, *Angew. Chem. Int. Ed. Engl.* **2013**, *52*, 6996–6999.
- [20] S. Walter, H. Spohr, R. Franke, W. Hieringer, P. Wasserscheid, M. Haumann, *ACS Catal.* **2017**, *7*, 1035–1044.
- [21] S. Werner, N. Szesni, R. W. Fischer, M. Haumann, P. Wasserscheid, *Phys. Chem. Chem. Phys.* **2009**, *11*, 10817–10819.
- [22] S. Werner, N. Szesni, M. Kaiser, M. Haumann, P. Wasserscheid, *Chem. Eng. Technol.* **2012**, *35*, 1962–1967.
- [23] J. Zhao, Y. Yu, X. Xu, S. Di, B. Wang, H. Xu, J. Ni, L. Guo, Z. Pan, X. Li, *Appl. Catal. B* **2017**, *206*, 175–183.
- [24] M. Logemann, P. Wolf, J. Loipersböck, A. Schrade, M. Wessling, M. Haumann, *Catalysis Science, Technology* **2021**, *11*, 1558–1570.
- [25] R. Franke, H. Hahn, *Evonik Elements* **2015**, 51.
- [26] A. Beckmann, F. J. Keil, *Chem. Eng. Sci.* **2003**, *58*, 841–847.
- [27] M. Schörner, P. Rothgänger, K. Mitländer, D. Wisser, M. Thommes, M. Haumann, *ChemCatChem* **2021**, *13*, 4192–4200.
- [28] S. Kokolakis, in *PhD Thesis – Kinetische Modellierung der Hydroformylierung von 1-Buten an rhodiumbasierten SILP-Katalysatoren*, Technische Universität Darmstadt, **2017**.
- [29] A. Jörke, T. Gaide, A. Behr, A. Vorholt, A. Seidel-Morgenstern, C. Hamel, *Chem. Eng. J.* **2017**, *313*, 382–397.
- [30] M. Eichmann, W. Keim, M. Haumann, B. U. Melcher, P. Wasserscheid, *J. Mol. Catal. A* **2009**, *314*, 42–48.
- [31] C. A. Ohlin, P. J. Dyson, G. Laurency, *Chem. Commun.* **2004**, 1070–1071.
- [32] A. Sharma, C. Julcour, A. A. Kelkar, R. M. Deshpande, H. Delmas, *Ind. Eng. Chem. Res.* **2009**, *48*, 4075–4082.
- [33] S. Walter, *PhD Thesis – Reaktionstechnische Untersuchungen an Supported-Ionic-Liquid-Phase (SILP) Katalysatoren zur Hydroformylierung von Buten und Verfahrensaspekte zur Umsetzung von n-Butan zu Aldehyden*, Friedrich-Alexander-Universität Erlangen-Nürnberg, **2015**.
- [34] L. Le Goanvic, J. Ternel, J.-L. Couturier, J.-L. Dubois, J.-F. Carpentier, *Catalysts* **2018**, *8*, 148.
- [35] R. M. Deshpande, A. A. Kelkar, A. Sharma, C. Julcour-Lebigue, H. Delmas, *Chem. Eng. Sci.* **2011**, *66*, 1631–1639.
- [36] R. M. Deshpande, R. V. Chaudhari, *Ind. Eng. Chem. Res.* **1988**, *27*, 1996–2002.
- [37] R. M. Deshpande, Purwanto, H. Delmas, R. V. Chaudhari, *Ind. Eng. Chem. Res.* **1996**, *35*, 3927–3933.
- [38] D. Y. Murzin, A. Bernas, T. Salmi, *J. Mol. Catal. A* **2010**, *315*, 148–154.
- [39] D. Y. Murzin, A. Bernas, T. Salmi, *AIChE J.* **2012**, *58*, 2192–2201.
- [40] G. Kiedorf, D. M. Hoang, A. Müller, A. Jörke, J. Markert, H. Arellano-García, A. Seidel-Morgenstern, C. Hamel, *Chem. Eng. Sci.* **2014**, *115*, 31–48.
- [41] A. C. J. Koeken, L. J. P. van den Broeke, B.-J. Deelman, J. T. F. Keurentjes, *J. Mol. Catal. A* **2011**, *346*, 1–11.
- [42] J. A. Christiansen, *Adv. Catal.* **1953**, *5*, 311–353.
- [43] F. G. Helfferich, in *Kinetics of multistep reactions, 2nd edition*, Elsevier, 2 edn., **2004**.
- [44] D. Evans, J. A. Osborn, G. Wilkinson, *J. Chem. Soc. A* **1968**, 3133–3142.
- [45] M. Boudart, *AIChE J.* **1972**, *18*, 465–478.
- [46] A. Jörke, A. Seidel-Morgenstern, C. Hamel, *J. Mol. Catal. a-Chem* **2017**, *426*, 10–14.
- [47] <https://www.macbeth-project.eu/> (accessed November 2021).
- [48] J. M. Marinkovic, in *Supported Ionic Liquid-Phase (SILP) Membrane Reaction Systems for Industrial Homogeneous Catalysis*, Ph.D thesis, DTU, Denmark, **2019**.

Manuscript received: January 17, 2022
Revised manuscript received: April 26, 2022
Version of record online: May 19, 2022